Journal of The Electrochemical Society, 164 (7) H491-H496 (2017)

Analysis of charge transport in $Ce_{0.8}Gd_{0.2-x}Pr_xO_{2-\delta}$ at $T \leq 600$ °C

Kerstin Neuhaus*[1], Sebastian Eickholt*[1], Aditya Maheshwari[1], Falk Schulze-Küppers[2], Stefan Baumann[2], Hans-Dieter Wiemhöfer[1]

[1] University of Münster, Institute of Inorganic and Analytical Chemistry, Corrensstraße 28/30, 48149 Münster, Germany
[2] Forschungszentrum Jülich, Institute of Energy and Climate Research, Materials Synthesis and Processing, Wilhelm-Johnen-Straße, 52452 Jülich, Germany

* Both authors contributed equally to the work.

Abstract

Doped ceria pellets with the composition $Ce_{0.8}Gd_{0.2-x}Pr_xO_{2-\delta}$ with x = 0.15, 0.1, 0.05, and 0.03 were investigated with a special focus on the partial conductivities in the temperature range of 200-600 °C. Temperature dependent conductivity provided by impedance spectroscopy in air was compared to measurements of the oxygen partial pressure dependent electronic conductivity. The electronic conductivity was analyzed down to 200 °C by using a modified Hebb-Wagner setup with encapsulated Pt microcontacts. A small polaron hopping process introduced by reduction of praseodymium was found to have a pronounced influence on the electronic conductivity at low temperatures. A splitting of the maximum introduced by praseodymium small polaron hopping was observed. Especially for the compositions $x \leq 0.1$, a strong deviation of the electronic conductivity curves from the standard acceptor doping case was measured due to superimposed electronic conductivity from the $Pr^{3+/4+}$ redox reaction.

1 Introduction

As a material which shows high oxygen ion conductivity paired with a significant electronic conductivity and a resulting high oxygen storage capacity, acceptor doped ceria has in the past been discussed and deployed for a variety of different applications. These applications range from high temperature regime applications like solid oxide fuel cell components [1, 2] and gas sensors [3] to applications at quite low temperatures like catalyst materials [4, 5] and the pharmaceutical field [6, 7]. Although its standard application temperature (500-800 °C) is already considerably lower than for the comparable yttria-stabilized zirconia [8], measurement data on the low temperature charge transport and especially on the low temperature behavior of the partial conductivities of doped ceria are sketchy. Nevertheless, an understanding of the low temperature behavior is vital for optimizing the use of ceria as a catalyst and oxygen storage material, which is becoming more and more industrially important [4, 9, 10].

In the last forty years, the conductivity of solely Gd [2, 8, 11, 12] or Pr doped ceria [13-16] as well as the co-doped system $Ce_{1-(x+y)}Gd_xPr_yO_{2-\delta}$ [17-21] or other acceptor dopant/Pr co-doped systems [22] have been well investigated in the high temperature regime above 600 °C. Especially co-doped systems are of high interest

for further improving the performance ceria-based materials especially for use in solid oxide fuel cells and for oxygen permeable membranes. In the case of Gd and Pr for instance, the strong volume change of purely Pr doped ceria with oxygen uptake and release can be reduced by co-doping with Gd [23]. Simultaneously, the increase of the electronic conductivity introduced by Pr doping can in large parts be preserved depending on the Gd/Pr ratio [17, 18].

In the work presented here, we evaluate data on the temperature dependent conduction behavior of Gd/Pr co-doped ceria with the compositions $Ce_{0.8}Gd_{0.2-x}Pr_xO_{2-\delta}$ with x = 0.15, 0.1, 0.05, and 0.03 at temperatures below 600 °C. The focus lies mainly on the effect of the dopant ratio variation and accompanying variations of the defect mobilities and Pr-induced small polaron hopping effects in the low temperature regime.

2 Experiments

2.1 Sample preparation

Powders of the composition $Ce_{0.8}Gd_{0.2-x}Pr_xO_{2-\delta}$ with x=0.15, 0.1, 0.05, and 0.03 were synthesized from the respective nitrate hydrates using a modified Pecchini method [18]. The resulting powders were calcined for 5 h at 700 °C in air. After ball milling for 2 h, the powders were uniaxially dry pressed into pellets. These were sintered subsequently at 1600 °C for 2 h. All samples were found to be single-phase fluorite materials by XRD check. Additionally, the sample composition was found to accord with the nominal composition by analyzation using inductively coupled plasma optical emission spectrometry (ICP-OES). The porosity of the samples was determined graphically by SEM measurements and was in the range of 4% for all samples. The grain sizes of the samples (cf. Tab. 1) were checked by light microscopy using the lineal intercept method by Nelson and Wurst [24].

2.2 Impedance spectroscopy

Impedance measurements in air were carried out as a function of temperature in ambient air using a Novotherm HT 1200 (NovoControl GmbH). Pt resinate paste (RP 070107, Heraeus GmbH) was applied directly on the sample pellets and was sintered at 850 °C before measurement to minimize any contact resistance. The paste electrodes were contacted by a Pt-sheet. An AC peak-to-peak amplitude of 40 mV was chosen. The experimental frequency dependence of the impedance was fitted using the software package ZView 3.1c (Scribner Associates, Inc.) with regard to the medium and high frequency range.

For fitting, an equivalent circuit with two resistors in series, which each have a constant phase element in parallel, was used [25]. One resistor/constant phase element can be assigned to bulk characteristics and one to grain boundary characteristics, respectively. Bulk (σ_b) and bulk conductivities (σ_{gb}) have the following connection:

$$R_{\mathrm{total}} = R_{\mathrm{b}} + R_{\mathrm{gb}} = \frac{n}{A} \cdot \left(\frac{1}{\sigma_{\mathrm{b}}} \cdot L_{\mathrm{b}} + \frac{1}{\sigma_{\mathrm{gb}}} \cdot L_{\mathrm{gb}} \right) = \frac{1}{\sigma_{\mathrm{t}}} \quad (2)$$

Here, *n* is the number of grains perpendicular to the electric field, *A* is the contact area, L_{g} is the average grain size (cf. Tab. 1), L_{gb} is the average size of the grain boundary which was in our case assumed to be 1 nm [26, 27]. The grain boundary conductivity was corrected with the factor $\frac{L_{\mathrm{gb}}}{L_{\mathrm{g}}}$ to calculate the corrected grain boundary conductivity σ_{gb}^{*} according to the brick layer model [26, 28]. Activation energies were calculated from Arrhenius diagrams of the respective conductivities.

Tab. 1 Sample thickness, contact diameter of the Pt contacts used for impedance measurements and average grain size (L_{g}) of the four different samples with the composition $Ce_{0.8}Gd_{0.2-x}Pr_xO_{2-\delta}$.

x	thickness / cm	diameter / cm	L_{g} / µm
0.03	0.190	0.647	2.9
0.05	0.198	0.647	4.0
0.10	0.198	0.647	2.9
0.15	0.187	0.621	2.4

2.3 Microcontact measurements

The electronic partial conductivity of the samples was investigated using a modified Hebb-Wagner setup with encapsulated platinum micro contact as working electrode and a Pt sheet as counter electrode. Measurements were conducted at temperatures between 800-200 °C. An extended description of the microcontact measurement method and the theoretical basis can be found in previous publications [17, 18, 29]. All voltage values were corrected with regard to the additional potential difference due to the contact resistance. The contact resistance was obtained by polarization with -0.5 and 0.1 V for each sample and subsequent open circuit measurements as described in [18].

The migration enthalpy ($H_{\mathrm{m,Pr}}$) of the Pr small polaron conductivity was calculated from the Pr peak conductivity values with the following equation:

$$\sigma_{\mathrm{e,max}}(T) = [\mathrm{Pr_{Ce}}] \cdot 0.5_{\mathrm{Pr'_{Ce}}} \cdot 0.5_{\mathrm{Pr^{\times}_{Ce}}} \cdot \frac{\overset{\circ}{\mu}_{\mathrm{Pr}}}{T^{\frac{3}{2}}} \cdot \mathrm{e}^{\left(-\frac{H_{\mathrm{m,Pr}}}{k_{\mathrm{B}} \cdot T}\right)} \quad (3)$$

The standard reaction enthalpy (H_{rPr}) was derived from the Pr oxygen redox equilibrium (4) under the assumption that the concentrations of all relevant defects at the peaks are fixed due to $x_{\mathrm{Pr'_{Ce}}}/x_{\mathrm{Pr^{\times}_{Ce}}} = 1$. The oxygen partial pressure was substituted with the corresponding applied voltage of the peak (*E*). The difference between two peak positons in volt is equal to the difference in eV assuming an oxygen activity of one.

$$\frac{[V_O^{\bullet\bullet}]\cdot[Pr_M']^2\cdot\sqrt{e^{\left(\frac{E\cdot 4F}{R\cdot T}\right)}}}{[O_O^{\times}]\cdot[Pr_M^{\times}]^2} = y_{rPr}\cdot e^{-\frac{H_{rPr}}{k_B\cdot T}} \quad (4)$$

3 Measurement results

3.1 Impedance spectroscopy

Impedance spectroscopy measurements were carried out in ambient air in a cycle from 800 °C down to room temperature and a second cycle back up to 800 °C. The results were found to be reproducible. The Pr dopant should be mainly present in the Pr^{4+} state, although for high temperatures, a low concentration of already reduced Pr^{3+} can be present as the oxygen partial pressure, at which Pr reduction takes place, increases with increasing temperatures.

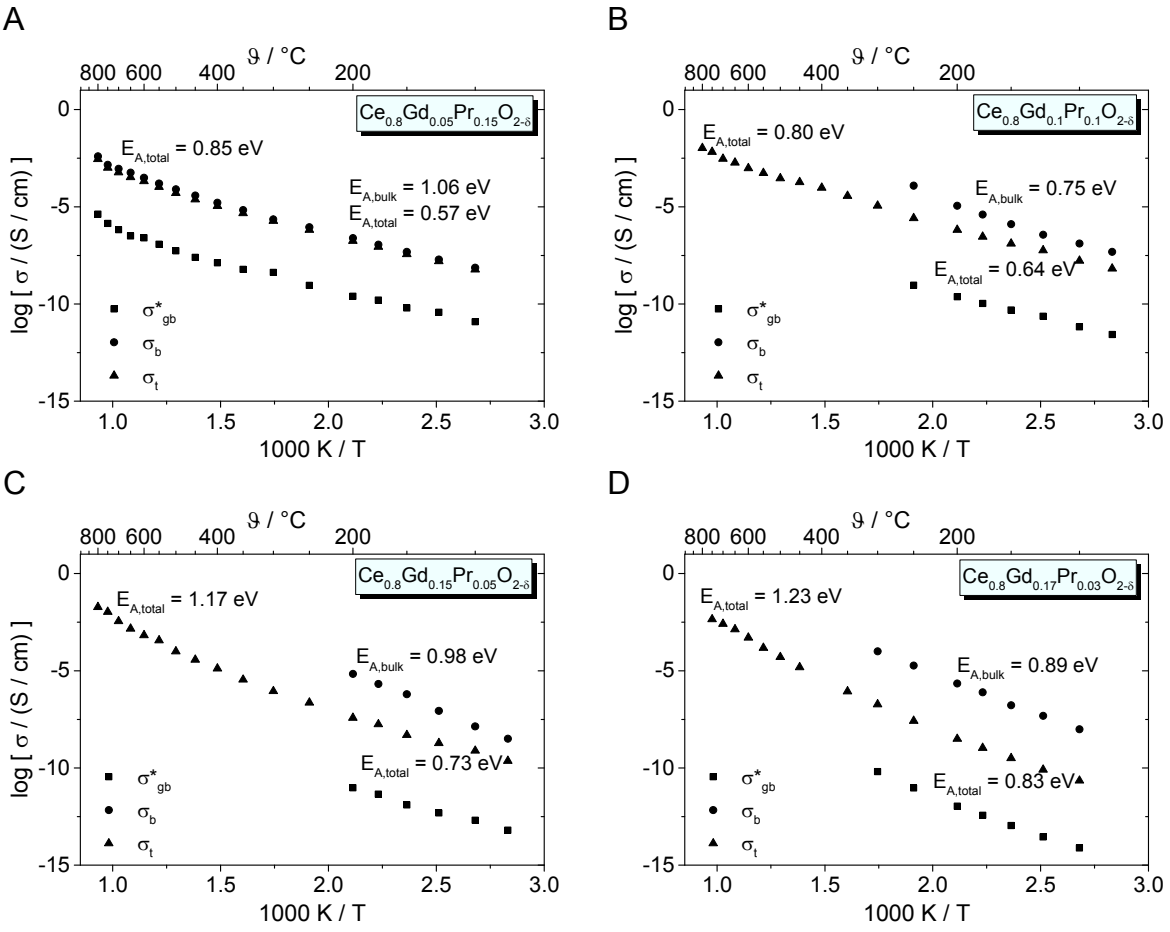

Fig. 1 Bulk and total conductivities of $Ce_{0.8}Gd_{0.2-x}Pr_xO_{2-\delta}$. Measurements were performed in ambient air.

It was only possible to distinguish the bulk conductivity contribution at low temperatures except for the case x = 0.15, as for higher temperatures, the contribution of bulk and grain boundaries became inseparable. So, for higher temperatures, only a value for the total conductivity (σ_t) is given (cf. Fig. 1). As can be

seen in Fig. 1, two different regimes can be distinguished from the activation energies derived from the total conductivity of the respective samples.

For all samples, $E_{A,total}$ was lower in the low temperature regime and increased gradually for higher temperatures, starting in the area of 400 °C. This is in discordance to previous publications, which found a slight increase of the activation energy below 400 °C for acceptor doped ceria [8, 20, 29]. The increase was ascribed to the development of defect associates at lower temperatures [8, 20, 29] which lower the ionic conductivity which is prevalent in acceptor doped materials.

For Pr doped ceria, this has to be regarded differently, though: in the high temperature regime, the total conductivity did not increase completely linearly with temperature but showed a slight S-curve (cf. Fig. 1) which is more pronounced for low Pr contents. The activation energies for the high temperature regime represent a value calculated from the line of best fit through the respective values.

The curving can be attributed to the influence of the Pr^{4+}/Pr^{3+} transition, although the electrons are only the minority charge carries in this material. The oxygen partial pressure at which the Pr^{4+} reduction occurs, decreases with increasing temperature and decreasing Pr content, leading to the observed nonlinearity. Altogether, the mixed conductivity is increased by increasing Pr addition.

Obviously, $E_{A,total}$ for high Pr concentration in the low temperature regime is the lowest and increases with increasing Gd/Pr ratio. At the same time, the measured conductivities especially in the low temperature regime are the highest for [Gd] = [Pr]. This sample also exhibits a minimum of $E_{A,bulk}$ and $E_{A,total}$ in the high temperature regime. The measured value of $E_{A,total}$ = 0.80 eV is consistent with the values by Steele [8] for $Ce_{0.8}Gd_{0.2}O_{2-\delta}$ ($E_{A,total}$ = 0.78 eV at 500-700 °C) and Ramesh [20] for $Ce_{0.84}Gd_{0.08}Pr_{0.08}O_{2-\delta}$ ($E_{A,total}$ = 0.79 eV at 500-700 °C).

3.2 Microcontact measurements

As can be seen from Fig. 2 to Fig. 5, below 600 °C the effect of small polaron hopping introduced by Pr substitution can be only detected for the compositions $x \leq 0.1$ for $Ce_{0.8}Gd_{0.2-x}Pr_xO_{2-\delta}$. For the composition x = 0.15, a “standard” behavior of the electronic conductivity with ±¼ slopes was found down to temperatures of 400 °C. This behavior can be attributed to the high Pr concentrations, which lead to a shift of the Pr small polaron hopping maximum to very low oxygen partial pressures. These oxygen partial pressures cannot be assessed with our measurement method.

In contrast, for the composition x = 0.1, an almost straight slope of the electronic conductivity curve can be found over nearly the whole oxygen partial pressure range. Only at 600 and 550 °C, a dip of the curve at low oxygen partial pressures indicate the position of the electronic conductivity minimum of this material. For the temperatures between 500 to 250 °C, only a very small slope of the curve can be

observed with a minimum in the partial pressure range of 0.001 to 0.01 bar oxygen partial pressure. This minimum shifts slightly to higher oxygen partial pressures with decreasing temperature. This behavior occurs due to the fact that the Pr induced conductivity maximum is superimposed on the “standard” +¼ curve.

The influence of the Pr small polaron hopping becomes most obvious for the composition with x = 0.05 and x = 0.03 (cf. Fig. 4 and Fig. 5). Here, an additional peak can be clearly observed in the range from 550 to 300 °C. The maximum is situated around 10^{-5} bar for 550 °C and rapidly moves to lower oxygen partial pressures as predicted. At 300 °C the position is around 10^{-20} bar and for the lower temperatures, the maximum is can be assumed outside of the measurement range of the shown measurements. Similarly to the observations made for x = 0.1, a minimum of the electronic conductivity can be found on the right-hand flank of the peak.

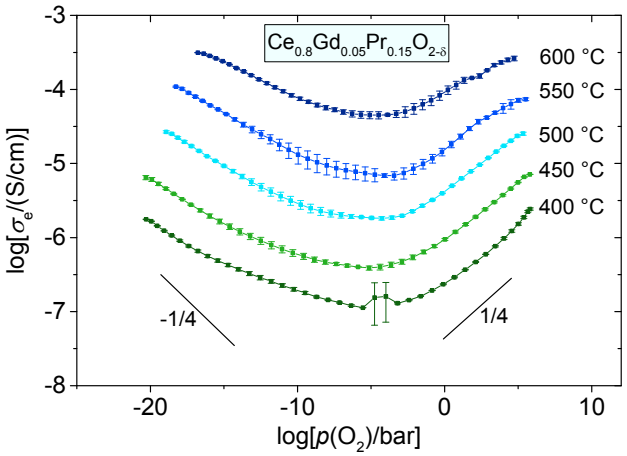

Fig. 2 Electronic conductivity of $Ce_{0.8}Gd_{0.05}Pr_{0.15}O_{2-\delta}$. Error bars show the standard deviation. Measurements below 400 °C were not evaluable.

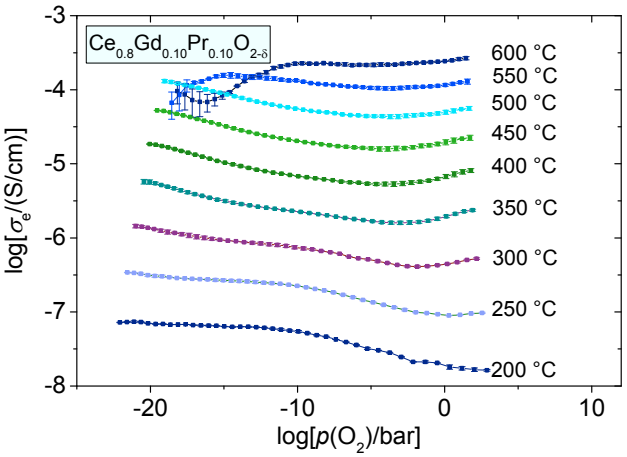

Fig. 3 Electronic conductivity of $Ce_{0.8}Gd_{0.1}Pr_{0.1}O_{2-\delta}$. Error bars show the standard deviation.

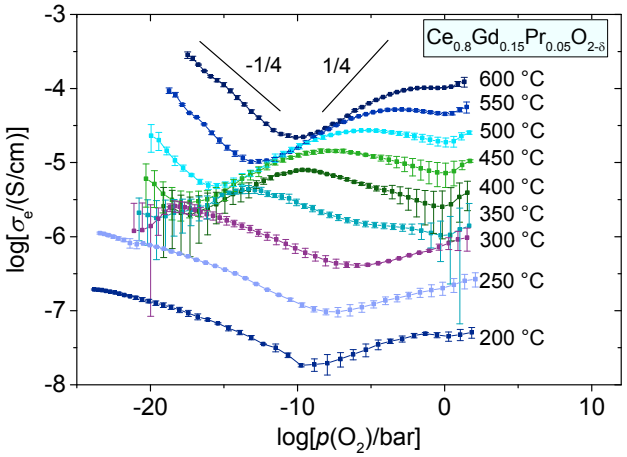

Fig. 4 Electronic conductivity of $Ce_{0.8}Gd_{0.15}Pr_{0.05}O_{2-\delta}$. Error bars show the standard deviation.

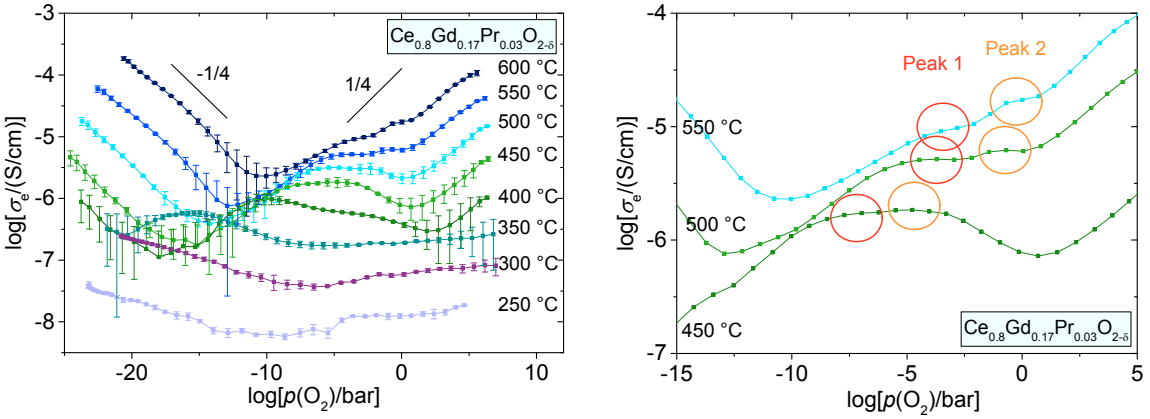

Fig. 5 Left hand side shows electronic conductivity of $Ce_{0.8}Gd_{0.17}Pr_{0.03}O_{2-\delta}$. Error bars show the standard deviation. The right graph shows an exemplary cutout where red and orange circles indicate the two different contributions to the observed maximum for $Ce_{0.8}Gd_{0.17}Pr_{0.03}O_{2-\delta}$. The error bars were left out for clarity.

In divergence to the findings by Bishop et al. [13, 15], two contributions of the Pr-induced maximum of the electronic conductivity could be distinguished at lower temperatures for Pr concentrations below 0.1 mol%. An example of the allocation of the two contributions to the Pr-induced maximum can be found in Fig. 5.

In Fig. 6 the $p(O_2)$ and temperature dependent allocation of the Pr-induced conductivity maximum is plotted for the compositions x = 0.1, 0.05, and 0.03. The values were taken from the measurements represented in Fig. 2 to

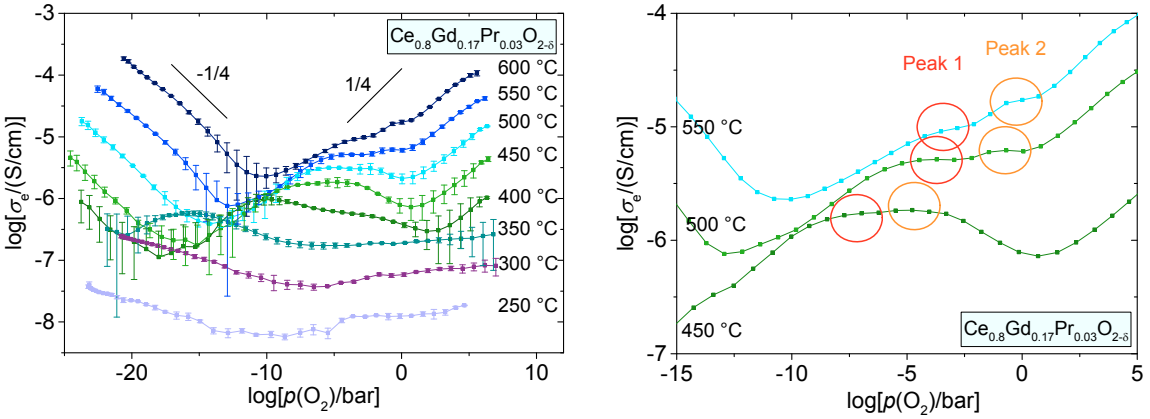

Fig. 5. For x = 0.1 and x = 0.05 a splitting of this maximum into distinct contributions can be observed in the intermediate to low temperature regime. For x = 0.03, a splitting into two contributions can be observed more or less over the whole temperature range.

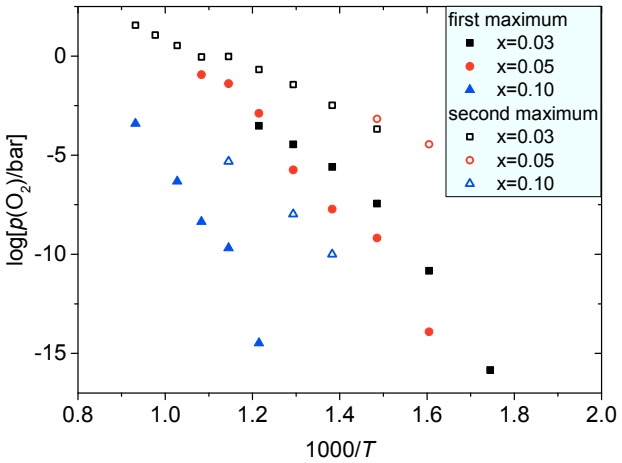

Fig. 6 Position of the first and the second Pr-induced maximum of the electronic conductivity for the compositions x= 0.1, 0.05, and 0.03. It becomes obvious that an increasing Gd-concentration pushes the point of Pr^{3+}/Pr^{4+}-equilibrium to higher oxygen partial pressures.

3.3. Calculations for Pr induced small polaron hopping

The enthalpy of reaction (H_r) of the Pr reduction and the enthalpy of migration ($H_{m,Pr}$) and the corresponding mobility pre-exponential (μ°_{Pr}) of the Pr induced small polaron hopping were calculated from the Pr-related peak which was found for the compositions x = 0.1, 0.05, and 0.03 (cf. eq. (3) and (4)). The derivations for calculation of these values can be found in the comprehensive work of Bishop et al. [13], where similar calculations were made for the composition $Ce_{0.9}Pr_{0.1}O_{2-\delta}$ at elevated temperatures, and in the work of Chatzichristodoulou et al. [30-32], where Pr in combination with Tb was investigated at temperatures between 600-900 °C. These publications are also referred to as comparison in the list of measured values in Tab. 2.

Tab. 2 List of calculated enthalpies of migration and enthalpies of reaction in eV and mobility pre-exponential in $cm^2\,K\,V^{-1}\,s^{-1}$ calculated from the maximum at lower oxygen partial pressures and comparison to literature values for $Ce_{0.9}Pr_{0.1}O_{2-\delta}$ (CPO10) [13] and $Ce_{0.8}Pr_{0.2}O_{2-\delta}$ (CPO20)

[30]. When possible, the low temperature range (200-400 °C) and high temperature range (400-800 °C) were distinguished. In case of splitted peaks, the enthalpies of reaction are given for both peaks. Values for peak 2 (located at higher oxygen partial pressure) are labeled with *.

	200-400 °C			400-800°C				
	This work			This work			[13]	[30]
x	0.03	0.05	0.1	0.03	0.05	0.1	CPO10	CPO20
H_{rPr}	-	-	-	-1.4/ -1.1*	-2.2	-2.9/ -1.9*	-	-
$H_{m,Pr}$	1.37	0.49	-	0.66	0.49	0.66	0.56 ±0.04	0.45 ±0.01
μ°_{Pr}	256 ±112	954 ±70	-	690 ±792	954 ±70	1262 ±537	801 ±300	147 ±1

It can be derived that the enthalpy of reduction increases with increasing Pr-content, for the first as well as the second Pr-induced peak. In contrast, the enthalpy of migration does not show such a clear behavior, but the values are in a similar value range as for $Ce_{0.9}Pr_{0.1}O_{2-\delta}$ published by Bishop et al. [13] and somewhat higher than for $Ce_{0.8}Pr_{0.2}O_{2-\delta}$ measured by Chatzichristodoulou and Hendriksen [30]. The pre-exponential factor is also relatively variable with large errors due to the mathematical fit of the data which is necessary to calculate this entity. A slight increasing trend of μ°_{Pr} with increasing Pr concentration could be estimated from the high temperature data.

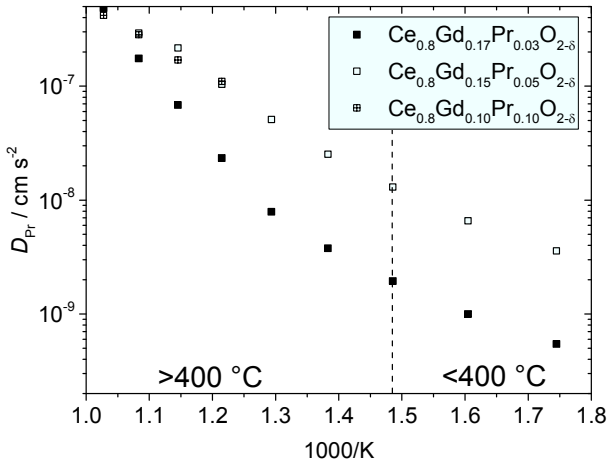

Fig. 7 Chemical diffusion coefficient for Pr small polaron hopping for the compositions $Ce_{0.8}Gd_{0.2-x}Pr_xO_{2-\delta}$ with x = 0.03, 0.05, 0.1.

Apart from the enthalpies of reaction and migration, a chemical diffusion coefficient D_{Pr} for the Pr^{3+}/Pr^{4+} small polaron hopping process was calculated for the compositions x = 0.1, 0.05 and 0.03 (cf. Fig. 7). D_{Pr} can be derived from the mobility at the maximum of electronic conductivity, as the diffusion coefficient is linearly dependent on the electronic mobility μ_{Pr} at a constant temperature:

$$\mu_{Pr}(T) = \frac{D_{Pr}}{T \cdot k_B} = \frac{\mu^{\circ}_{Pr}}{T} \cdot e^{\left(-\frac{H_{m,Pr}}{k_B \cdot T}\right)} \quad (5)$$

A calculation of D_{Pr} over the whole temperature range was only possible for x = 0.05 and 0.03. As can be seen from Fig. 7, the diffusion coefficient for x = 0.03 is considerably lower than for the other two compositions. At the same time, it can be observed that the curve progression of x = 0.1 and 0.05 is quite similar in the temperature range above 400 °C. Thus, we assume, that the diffusion coefficients for low temperatures for x = 0.1 and 0.15 can be extrapolated taking into account the measurements for x = 0.05. Obviously, above $[Pr^{3+/4+}] \approx 5$ mol% the Pr concentration does not determine the small polaron hopping velocity as much as the temperature, while for lower Pr concentrations, $[Pr^{3+/4+}]$ is also rate determining.

3.4 Discussion

Measurements of the total conductivity of the samples showed the expected behavior with an increase of the total activation energy in the range of 300 to 400 °C which can be attributed to dissipation of defect associates with increasing temperatures. A minimum of the total activation energy was found for 15 mol% Pr concentration. The sample with x = 0.1 showed the highest total conductivities, especially in the low temperature regime.

Tab. 3 presents the transference number for electrons $\frac{\sigma_e}{\sigma_t} = t_e$ for the four samples at a temperature of 300-500 °C in ambient air. It can be seen, that t_e increases with decreasing temperature for low Pr contents (x = 0.03 and 0.05), while for high Pr contents (x = 0.1 and 0.15), t_e decreases with decreasing temperature. To explain this behavior, several factors have to be taken into account, which are associated with the nonlinear influence of the variable Pr and Gd concentrations on the electron conductivity with temperature.

For the samples with Pr < 10 mol%, the behavior is clearly governed by the high Gd content, so the oxygen conductivity is prevalent within the high temperature regime while at low temperatures, the conduction behavior is controlled by the electron conductivity. For the samples with ≥ 10 mol%, the conduction behavior is governed by Pr where especially at high temperatures the mixed conductivity is increased.

Tab. 3 Transference numbers for electrons (t_e) at 500-300 °C in ambient air.

θ	x = 0.03	x = 0.05	x = 0.10	x = 0.15
500 °C	0.042	0.190	0.194	0.320
400 °C	0.097	0.210	0.071	0.027
300 °C	0.313	0.912	0.039	-

As described initially, Gd works as a pure acceptor dopant in ceria while the redox-activity of Pr triggers a small polaron hopping process when part of the Pr dopant get reduced at lower oxygen partial pressures. In our work, for samples with [Pr] ≤ 10 mol%, a splitting of the Pr-induced maximum into two distinct contributions

was observed especially for low temperatures. This split becomes more intense with decreasing Pr content.

Following the explanation by Ahn et al. [33], this could be attributed to whether the oxygen vacancies created by the polarization during the measurement of the electronic conductivity are located with two Pr ions or one Ce and one Pr as nearest neighbors.. The peak at the higher oxygen partial pressure (peak 2 in Fig. 5) could according to Ahn et al. be ascribed to the Pr-Pr case, while the peak at lower oxygen partial pressures (peak 1 in Fig. 5) could be assigned to the Pr-Ce case. The observation of the peaks being more distinct for low temperatures and low Pr contents makes sense, as the Pr-Ce case becomes more frequent and is not entirely overlain by the effect of oxygen vacancy creation with two Pr as nearest neighbors, which would be more favorable according to Ahn et al. [33]. In contradiction to our experiments the splitting of the Pr-induced conductivity maximum should then become more likely with increasing Pr content.

Therefore, we propose as another plausible explanation that the splitting of the maximum could be introduced by simultaneous reduction of Pr^{4+} and a breakup of defect accumulates composed of Pr ions and oxygen vacancies. The oxygen vacancy concentration increases with increasing Gd content, so a more pronounced splitting with decreasing Pr concentration could be explained by a higher abundance of oxygen vacancies for accumulate formation.
For all samples it was observed, that at very low temperatures (300 to 200 °C) the slope of the electronic conductivity was not following the ±¼ slope, which is predicted by Fig. 5. This is due to several problems in the experimental procedure, as initially stated: on the one hand, the measurement time did not allow for a complete polarization of the samples at these temperatures anymore, leading to lower conductivity values than anticipated, especially for high or very low $p(O_2)$. On the other hand, the contact resistance between micro contact and sample becomes very high, and although the electronic conductivity data were corrected for contact resistance, the contact resistance measured by polarization-relaxation measurements is generally underestimated as far as our experience goes, which leads to a similar effect. The electronic conductivity data for these temperatures can therefore be regarded as experiment-based low-case estimate for the actual conductivity.

4 Conclusion and Outlook

The measurements presented in this work clearly show that the electrochemical behavior of the samples with Gd/Pr co-doping is easily predictable by applying existing theoretical models. The effect of Pr as a redox active constituent is especially important for applications in the intermediate temperatures, as we were able to show that the maximum of electronic conductivity introduced by Pr small polaron hopping is situated in a technically accessible oxygen partial pressure regime for these temperatures. At the same time, the fixation of a certain number of oxygen vacancies

by using an additional acceptor dopant was found to be crucial for a reasonable total conductivity at low temperatures. These insights could be put to use for optimization of ceria-based low temperature materials e.g. for intermediate temperature SOFCs or for catalyst applications.

A major drawback of Pr-doped systems is their severe expansion behavior depending on variable oxygen partial pressures, but this behavior is not pronounced at temperatures below 500 °C, making Gd/Pr co-doped materials an interesting candidate for a number of different applications where mixed conductors are necessary.

5 Acknowledgements

The authors from University of Münster gratefully acknowledge funding by the Deutsche Forschungsgemeinschaft (DFG) within the collaborative project "CeO_2 based oxides as redox active materials for exchange and storage of oxygen" (2012-2015, grant# WI952/9-1).

6 Literature

1. Inaba, H. and H. Tagawa, *Ceria-based solid electrolytes - Review.* Solid State Ionics, 1996. **83**(1-2): p. 1-16.
2. Kharton, V.V., et al., *Ceria-based materials for solid oxide fuel cells.* J Mater Sci, 2001. **36**: p. 1105-1117.
3. Stefanik, T.S. and H.L. Tuller, *Ceria-based gas sensors.* J Eur Ceram Soc, 2001. **21**(10–11): p. 1967-1970.
4. Aneggi, E., et al., *Insights into the redox properties of ceria-based oxides and their implications in catalysis.* J Alloy Comp, 2006. **408–412**(0): p. 1096-1102.
5. Trovarelli, A., *Catalytic Properties of Ceria and CeO2-Containing Materials.* Catal Rev, 1996. **38**(4): p. 439-520.
6. Tarnuzzer, R.W., et al., *Vacancy Engineered Ceria Nanostructures for Protection from Radiation-Induced Cellular Damage.* Nano Lett, 2005. **5**(12): p. 2573-2577.
7. Patil, S., et al., *Protein adsorption and cellular uptake of cerium oxide nanoparticles as a function of zeta potential.* Biomater, 2007. **28**(31): p. 4600-4607.
8. Steele, B.C.H., *Appraisal of $Ce_{1-y}Gd_yO_{2-y/2}$ electrolytes for IT-SOFC operation at 500°C* Solid State Ionics, 2000. **129**(1-4): p. 95-110.
9. Trovarelli, A., et al., *The utilization of ceria in industrial catalysis.* Catal Today, 1999. **50**(2): p. 353-367.
10. Boaro, M., et al., *The use of temperature-programmed and dynamic/transient methods in catalysis: characterization of ceria-based, model three-way catalysts.* Catal Today, 2003. **77**(4): p. 407-417.
11. Fagg, D.P., V.V. Kharton, and J.R. Frade, *P-Type Electronic Transport in $Ce_{0.8}Gd_{0.2}O_{2-\delta}$: The Effect of Transition Metal Oxide Sintering Aids* Journal of Electroceramics, 2002. **9**(3): p. 199-207.
12. Tianshu, Z., et al., *Ionic conductivity in the CeO2-Gd2O3 system (0.05<=Gd/Ce<=0.4) prepared by oxalate coprecipitation.* Solid State Ionics, 2002. **148**(3-4): p. 567-573.

13. Bishop, S.R., T.S. Stefanik, and H.L. Tuller, *Electrical conductivity and defect equilibria of $Pr_{0.1}Ce_{0.9}O_{2-\delta}$.* Phys Chem Chem Phys, 2011. **13**(21): p. 10165-10173.
14. Kim, J.J., et al., *Optically derived energy band gap states of Pr in ceria.* Solid State Ionics, 2012. **225**: p. 198-200.
15. Tuller, H.L., et al., *Praseodymium doped ceria: model mixed ionic electronic conductor with coupled electrical, optical, mechanical and chemical properties.* Solid State Ionics, 2012. **225**: p. 194-197.
16. Takasu, Y., T. Sugino, and Y. Matsuda, *Electrical conductivity of praseodymia doped ceria.* J Appl Electrochem, 1984. **14**: p. 79-81.
17. Lübke, S. and H.-D. Wiemhöfer, *Electronic conductivity of Gd-doped ceria with additional Pr-doping.* Solid State Ionics, 1999. **117**(3–4): p. 229-243.
18. Schmale, K., et al., *Electronic conductivity of $Ce_{0.8}Gd_{0.2-x}Pr_xO_{2-\delta}$ and influence of added CoO.* Phys Stat Sol B, 2011. **248**(2): p. 314-322.
19. Torrens, R., N.M. Sammes, and G. Tompsett, *Characterization of Pr- and Sm-Doped $Ce_{0.8}Gd_{0.2}O_{2}$™.* J Electroceram, 2004. **13**(1): p. 683-689.
20. Ramesh, S. and K.C. James Raju, *Preparation and characterization of $Ce_{1-x}(Gd_{0.5}Pr_{0.5})_xO_2$ electrolyte for IT-SOFCs.* Int J Hydrogen Energ, 2012. **37**(13): p. 10311-10317.
21. Kharton, V.V., et al., *Electron–hole conduction in Pr-doped $Ce(Gd)O_{2-\delta}$ by faradaic efficiency and emf measurements.* Electrochim Acta, 2001. **46**(18): p. 2879-2889.
22. Ji, Y., et al., *The effect of Pr co-dopant on the performance of solid oxide fuel cells with Sm-doped ceria electrolyte.* J Alloy Compd, 2005. **389**(1–2): p. 317-322.
23. Heidenreich, M., et al., *Expansion behaviour of (Gd, Pr)-substituted CeO_2 in dependence on temperature and oxygen partial pressure.* Solid State Ionics, 2015. **283**: p. 56-67.
24. Wurst, J.C. and J.A. Nelson, *Lineal Intercept Technique for Measuring Grain Size in Two-Phase Polycrystalline Ceramics.* J Am Ceram Soc, 1972. **55**(2): p. 109-109.
25. Schmale, K., et al., *Influence of zinc oxide on the conductivity of ceria.* Journal of The Electrochemical Society, 2013. **160**(9): p. F1081-F1087.
26. Jasper, A., J.A. Kilner, and D.W. McComb, *TEM and impedance spectroscopy of doped ceria electrolytes.* Solid State Ionics, 2008. **179**(21): p. 904-908.
27. Hwang, J.-H., D.S. McLachlan, and T.O. Mason, *Brick Layer Model Analysis of Nanoscale-to-Microscale Cerium Dioxide.* J Electroceram, 1999. **3**(1): p. 7-16.
28. Christie, G.M. and F.P.F. Van Berkel, *Microstructure—ionic conductivity relationships in ceria-gadolinia electrolytes.* Solid State Ionics, 1996. **83**(1): p. 17-27.
29. Eufinger, J.-P., et al., *The model case of an oxygen storage catalyst–non-stoichiometry, point defects and electrical conductivity of single crystalline CeO_2–ZrO_2–Y_2O_3 solid solutions.* Phys Chem Chem Phys, 2014. **16**(46): p. 25583-25600.
30. Chatzichristodoulou, C. and P.V. Hendriksen, *Electronic and Ionic Transport in $Ce_{0.8}Pr_xTb_{0.2-x}O_{2-\delta}$ and Evaluation of Performance as Oxygen Permeation Membranes.* J Electrochem Soc, 2012. **159**(11): p. E162-E170.
31. Chatzichristodoulou, C., P.V. Hendriksen, and A. Hagen, *Defect Chemistry and Thermomechanical Properties of $Ce_{0.8}Pr_xTb_{0.2-x}O_{2-\delta}$.* J Electrochem Soc, 2010. **157**(2): p. B299.

32. Chatzichristodoulou, C., et al., *Oxygen Nonstoichiometry and Defect Chemistry Modelling of $Ce_{0.8}Pr_xTb_{0.2-x}O_{2-\delta}$.* 2008: p. 347-359.
33. Ahn, K., et al., *Role of Multivalent Pr in the Formation and Migration of Oxygen Vacancy in Pr-Doped Ceria: Experimental and First-Principles Investigations.* Chem Mater, 2012. **24**(21): p. 4261-4267.